chemosensors

MDPI

Article

Prediction of Diamene-Based Chemosensors

Danil W. Boukhvalov [1,2,*] and Vladimir Yu. Osipov [3]

[1] College of Science, Institute of Materials Physics and Chemistry, Nanjing Forestry University, Nanjing 210037, China
[2] Institute of Physics and Technology, Ural Federal University, Mira 19 Str., 620002 Yekaterinburg, Russia
[3] Ioffe Institute, Polytechnicheskaya 26, 194021 St. Petersburg, Russia
* Correspondence: danil@njfu.edu.cn

Abstract: This paper presents the results of systematic studies of the atomic structure of the layered bulk, bilayer, and monolayer of diamene (a two-dimensional diamond monolayer recently synthesized by various methods) functionalized with fluorine and hydroxyl groups with the chemical formulas C_2F and C_2OH. The results of our calculations show that both types of diamene under discussion have a wide optical gap corresponding to the absorption of light in the UV spectral range. The formation of a boundary between these two types of diamene layers leads to a significant decrease in the band gap. Therefore, this layered material, with an interface between fluorinated and hydroxylated diamenes (C_2F/C_2OH structures), can be considered a suitable material for converting UV radiation into visible light in the orange-yellow part of the spectrum. The adsorption of acetone or water on the C_2F/C_2OH structures results in visible changes in the band gap. The effect on photoemission is different for different detected analytes. The presence of formaldehyde in water ensures the appearance of distinct peaks in the absorption spectra of structures based on C_2F/C_2OH. Our simulation results suggest that the simulated C_2F/C_2OH structures can be used as chemically stable, lightweight materials composed of common elements for a highly selective chemical sensor in liquid and air.

Keywords: 2D materials; volatile organic compounds; formaldehyde; acetone; humidity; downconversion

Citation: Boukhvalov, D.W.; Osipov, V.Y. Prediction of Diamene-Based Chemosensors. *Chemosensors* **2022**, *10*, 480. https://doi.org/10.3390/chemosensors10110480

Academic Editor: Eleonora Alfinito

Received: 12 October 2022
Accepted: 8 November 2022
Published: 15 November 2022

1. Introduction

In the last decade, luminescent sensor materials have been widely discussed both experimentally [1–3] and theoretically [4–6]. The advantages of this class of materials are the stability of the sensing characteristics in external electric and magnetic fields and the possibility of separating the sensitive and detecting parts of the device [7,8]. The latter property makes it possible to use luminescent sensor materials in remote areas and/or in hazardous environments. Complex compounds with lanthanides are usually considered promising for use as luminescent sensor materials [7,9]. In addition to the rarity and cost of the lanthanides, another disadvantage of these compounds is the deterioration of perceptual characteristics in a humid environment. Thus, it is necessary to develop an alternative effective luminescent sensing material that is reliable in various harsh and humid conditions and is built from common elements.

When stability is essential, diamonds are an obvious choice for transparent materials. Bulk diamonds are less commonly used as sensors. However, thin diamond layers and submicron diamond particles can be used to design sensors. Thus, diamond particles 50–100 nm in size with nitrogen-vacancy fluorescent centers have recently been used for local determination of the pH of the medium inside biological cells in real time using the method of optically detected magnetic resonance [10]. Thin layers based on diamond-like carbon or nanocrystalline diamond can be used as carriers of grafted molecular structures—sensitive molecules that can be used as sensors. For example, a diamond surface terminated by atomic hydrogen can be used to design gas sensors [11]. In the latter case, the change

in the electrical properties of the surface during the sorption of external agents from the atmosphere is monitored. The surface of a diamond can also be a carrier of grafted hydrophobic polymer structures that facilitate the separation of the studied analyte in the sensor from the aqueous medium [12]. In this case, infrared absorption spectroscopy in the total internal reflection mode is used to study the analyte absorbed inside the polymer. In turn, diamond doped with boron can act as an electrode for a number of inert electrochemical sensors with nanomolar threshold sensitivity [13,14]. The advantage of the diamond lattice is its inertness to external agents and environments.

Two-dimensional diamonds (see Figure 1a,b) or diamenes were initially predicted theoretically [15] and, decades later, synthesized in several experiments by different research groups [16,17] (for review, see Ref. [18]). Functional groups on the surface play essential roles in the stabilization of 2D-diamond morphology. Experimental works demonstrate that hydrogenation of the surface allows for the formation of structures that are stable only under high pressure [19]. On the contrary, diamene, with its surface functionalized with fluorine and hydroxyl groups, is rather stable material [18]. Theoretical simulations [15] and experimental measurements [17] demonstrate that diamenes have a wide energy gap. The combination of the energy gap corresponding with the UV part of the spectra with stable and uniform atomic structure makes diamene a prospective wide-gap material for the optical [20] and chemical [21] sensors.

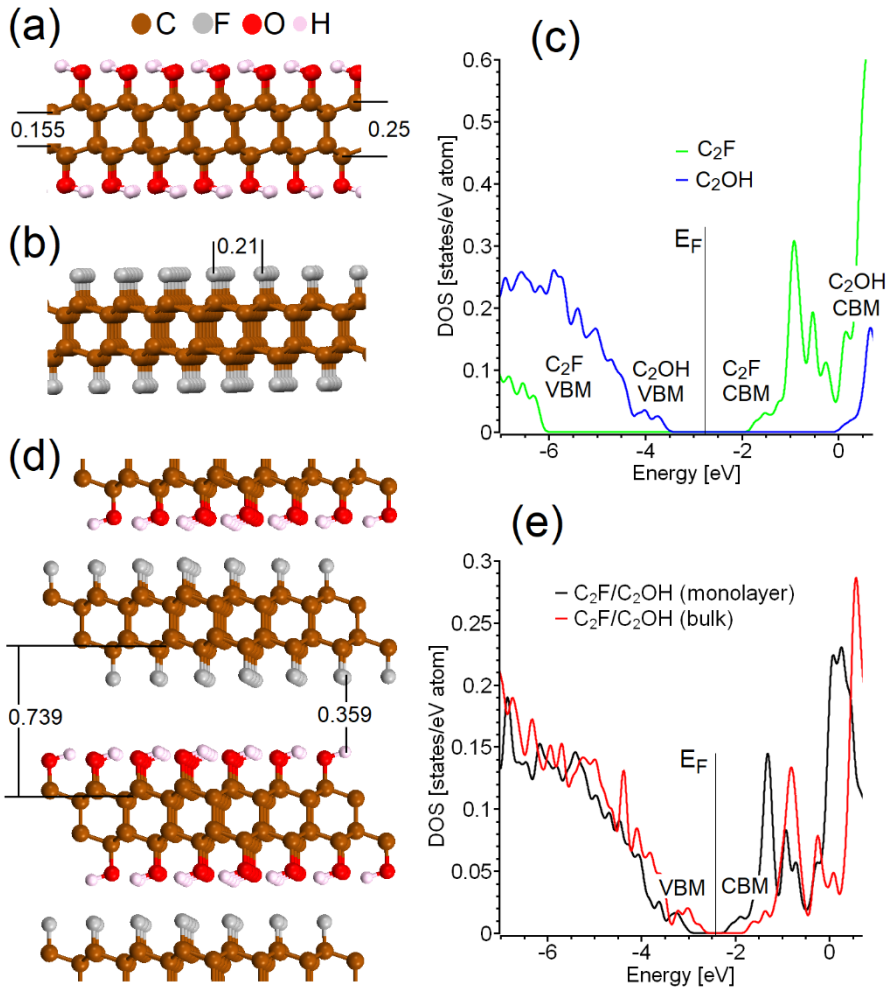

Figure 1. Side view of optimized atomic structure of diamenes C_2OH (**a**), C_2F (**b**), and part of bulk diamene with alternating C_2F/C_2OH structure (**d**). On the right are corresponding total densities of states of C_2OH and C_2F monolayers (**c**) and C_2F/C_2OH-structure in bulk (**e**) and single C_2F/C_2OH-layer form. All distances on panels (**a**,**b**,**d**) are reported in nanometers. E_F is a Fermi energy.

In this paper, we report the results of the simulations of the atomic and electronic structure of the interface between the layers of diamene functionalized by fluorine and the layers of diamene functionalized by hydroxyl groups. We studied the suitability of these compounds for probing in air and liquid. Because the presence of acetone in exhaled air is important for diagnosing early stage diabetes [22], we modeled the adsorption of acetone from the air on diamene-based compounds. To test the effect of moisture and liquid media, the interaction of these compounds with water was simulated. To evaluate the effectiveness of diamene-based compounds as sensors in liquid media, we simulated the interaction of formaldehyde [23] in aqueous media with diamene-based compounds.

2. Computational Methods

Theoretical modeling was carried out using SIESTA pseudopotential code [24] employing the generalized gradient approximation (GGA-PBE) [25] for the exchange-correlation potential in a spin-polarized mode. Van der Waals correction was also taken into account using the approach proposed by Dion et. al. [26] implemented in SIESTA code. A full optimization of the atomic positions was carried out, during which the electronic ground state was consistently found using norm-conserving pseudopotentials [27] for the cores with a double-ξ-plus polarization basis for the localized orbitals of nonhydrogen atoms and a double ξ for hydrogen atoms. Note that the used basis corresponded with a minimal basis set superposition error (BSSE) [28]. Note that the typical van der Waals bonds contribution from BSSE is about 5 K or 0.42 meV [29], which is three orders smaller than the values of energy calculated for these systems. The force and total energy were optimized with an accuracy of 0.04 eV $Å^{-1}$ and 1.0 meV/cell (or less than 0.02 meV/atom), respectively. The values of transferred charge were calculated by Bader analysis.

In this paper, we discuss the relationships between atomic structures of various simulated systems and the value of the energy gap between the valence band maximum (VBM) and conductive band minimum (CBM) in the analyzed periodic systems. The value of this band gap determines the wavelength of the characteristic fluorescence/luminescence—more precisely, its lower limit (in the approximation of the absence of the energy states associated with intrinsic defects in the band gap). In practice, luminescence is excited by optical short-wavelength laser radiation. This kind of luminescence is called photoluminescence (PL). The standard DFT realized in used computational code provides an underestimation of the values of the bandgap. [30] In the mentioned work, the simple linear relationship between the measured (E_{exp}) and calculated within standard DFT (E_{DFT}) values of the bandgap (in the range from 0 to 7 eV) were reported. Relationships between empirical values of bandgaps and those calculated within DFT frameworks can be approximated by a semiempirical formula:

$$E_{expt} = 0.8\ eV + 1.1E_{DFT} \quad (1)$$

We used this formula to estimate the correct values of the bandgaps based on the results of our DFT calculations.

The values of interlayer binding energies were calculated by the following standard formula:

$$E_{bind} = (E_{m1} + E_{m1} - E_{inter})/n \quad (2)$$

where E_{m1} and E_{m2} are the calculated total energies of the free-standing isolated monolayers forming the interface when in contact, E_{inter} is the calculated total energy of the resulting interface, and n is the number of interlayer interactions for each unit of monolayer. The value of n is equal to one for a bilayer and two for a monolayer. Note that positive binding energy corresponds to stable interfaces. The enthalpy of adsorption was calculated by a similar standard formula:

$$E_{ads} = E_{host+guest} - (E_{host} + E_{guest}) \quad (3)$$

where E_{host}, E_{guest}, and $E_{host+guest}$ are the total energies of the substrate, analyte, and substrate with adsorbed analyte, respectively.

3. Results and Discussion

3.1. Atomic Structure and Physical Properties of C_2F/C_2OH Interface in Air

The first step in our modeling was the construction of models of diamond-like C_2F and C_2OH monolayers. For this, we used a unit cell of two-layer graphene with AB stacking under periodic boundary conditions. Two carbon atoms located one above the other were initially slightly (by 0.1 Å) shifted toward each other to initiate the formation of an interlayer covalent bond. The carbon atoms belonging to another sublattice were displaced in opposite directions with the addition of fluorine atoms or hydroxyl groups to these carbon atoms. After that, complete optimization of the lattice parameters and the positions of atoms was carried out. The results of the DFT calculations are shown in Figure 1a,b. All carbon atoms in these structures are located in a tetrahedral environment, which corresponds to sp^3 hybridization. Half of the carbon atoms in each sublayer of the diamene are bonded to only carbon atoms. The other half of the carbons consist of three carbons from the same sublayer and one surface functional group. The distance between the nearest average parallel lines passing through the centers of functional groups is about 0.21 nm, and the interlayer distance is about 0.74 nm with an interlayer distance of 0.36 nm (see Figure 1a,b,d). Note that the first value (0.21 nm) matches well with the period of straight bands observed in some carbon nanostructures [31]. Thus, we also assumed the possibility of the formation of some diamene-like structures during the production of carbon dots. Thus, the atomic structure of some carbon dots known from the literature should be considered, taking into account the possibility of the formation of diamene-like structures. Note that the methods used to produce the mentioned carbon dots are considerably simpler than the modern methods for the fabrication of diamenes (see Introduction).

Because almost all carbon atoms in these systems have sp^3 hybridization, the electronic structure of both systems has a diamond-like character (see Figure 2c). The key difference between the two discussed systems (C_2F and C_2OH) lies in the absolute positions of the valence band maximum (VBM) and conduction band minimum (CBM) on the energy scale. The formation of the interface between these two compounds allows for the transfer of photogenerated electrons from CBM C_2OH (about 0 eV) through the interface into the C_2F conductive band with a CBM of about −1.8 eV. A photogenerated hole from the top of the C_2F valence band (about −6 eV) moves through the interface to the C_2OH valence bands with a maximum of about −3.5 eV (see Figure 1c), and further radiative recombination occurs. To estimate the energy characteristics of the emitted photons, we simulated the boundary between C_2F- and C_2OH-terminated atomic layers (see Figure 1d) and estimated the energy gap of the material under discussion. The calculated density of states of the C_2F/C_2OH interface (see Figure 1e) confirmed this initial assumption. The calculated value of the band gap is about 1.2 eV. Taking into account the underestimation of the band gap in the standard DFT framework, estimated by Formula (1), the energy of the emitted photon is about 2.1 eV, which corresponds to a wavelength of about 590 nm and lies in the orange-yellow part of the visible spectrum. Therefore, C_2F/C_2OH interfaces can be considered suitable materials for converting absorbed UV radiation into visible light in the orange-yellow part of the spectrum. Thus, diamene, like other wide-gap [15] materials, can be used to convert UV radiation into visible radiation.

The implementation of the scenario considered above is possible only in the presence of charge transfer between parts of the interface (for a detailed discussion and experimental evidence, see Ref. [32]). Similar to the work cited above, we calculated the change in the charge density after the formation of the interface between the C_2F and C_2OH monolayers. The calculation results (Figure 2a) demonstrate a visible change in the charge density map across the interface, which is direct evidence of charge transfer between the C_2F and C_2OH monolayers. The value of the transferred charge is about -0.03 e^- per unit cell. Note that the hopping of the electrons across the interface requires overlap between CBM-related

bands of neighboring layers in the coordinate space. The visualization of these bands (see Figure 2b) demonstrates the presence of this overlap. An almost identical picture (omitted due to similarity) could be observed for the overlap between the bands corresponding with VBM of both constituents of the interface. Therefore, the conversion of UV/blue light to the longer wavelength of visible light discussed above is possible.

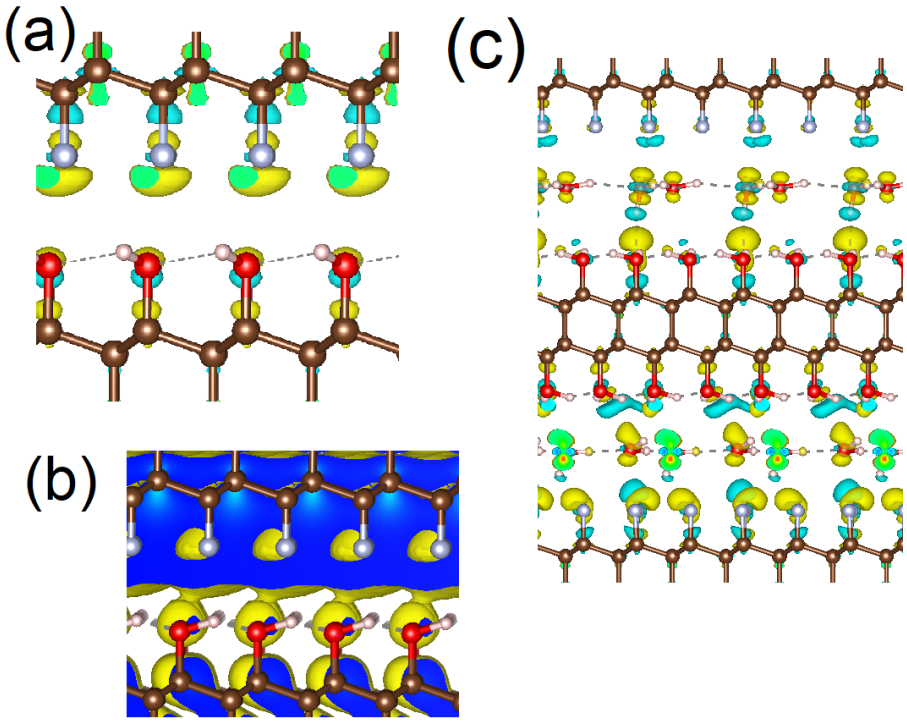

Figure 2. Changes in charge density after formation of C_2F/C_2OH interface (**a**), the sequence charge density of conductive band minimum orbitals of C_2F and C_2OH in C_2F/C_2OH interface (**b**), and changes in charge density after formation of multilayered water–C_2F–water–C_2OH–water structure (**c**). Cyan and yellow clouds corresponding with decreasing and increasing charge density. The color scale of the atoms is the same as in Figure 1.

The next step in our simulation was to test the effect of the formation of a bulk structure from alternating C_2F and C_2OH monolayers (see Figure 1d). The calculated atomic structure of the C_2F/C_2OH bulk structure is similar to that obtained from the calculations for a single layer. The formation of an infinite alternation of C_2F and C_2OH layers leads to insignificant changes in bandwidth values, so the color of the emitted light does not depend on the number of layers in the system. Because the fabrication of the bulk structures based on C_2F/C_2OH by precipitation is much easier than that of single-layer C_2F/C_2OH, the production of bulk devices based on diamene can be considered a realistic proposal.

The next step in our modeling of C_2F/C_2OH interfaces was the assessment of the chemical and structural stability of the system. The calculated energies of removal of one fluorine atom or a single hydroxyl group from the surface of the C_2F/C_2OH are approximately 2.5 eV and 1.8 eV, respectively. Therefore, thermal degradation of C_2F/C_2OH-based materials requires a temperature of hundreds of degrees Celsius (see reference discussion in [33]). The binding energies calculated by Formula (2) between the C_2F and C_2OH monolayers are 0.22 and 0.46 meV/unit for the C_2F/C_2OH bilayer and bulk, respectively. Note that the energies obtained are typical for hydrogen bonds (about 0.15 eV/bond) [34] and higher than those calculated for interlayer bonds in graphite (0.04 eV/bond) [35]. Thus, spontaneous delamination of layers in structures based on C_2F/C_2OH at room temperature can be considered unlikely at temperatures below several hundred degrees Celsius.

3.2. Atomic Structure and Physical Properties of C_2F/C_2OH-Interface in Liquid Media

The C_2F/C_2OH interface described in the previous section can be considered an interface between hydrophobic (C_2F) and hydrophilic (C_2OH) surfaces. Known experimental results demonstrate the possibility of water intercalation between such interfaces, with the formation of hexagonal ice in the interlayer space [36,37]. To test this scenario, we increased the supercell along the layers and then quasirandomly placed several water molecules between and above the layers. Similar to previous works [36,38], the formation of a monolayer of hexagonal ice was observed (see Figure 3a,b). Note that the ordering of water molecules in hexagonal ice was obtained by optimizing quasirandomly distributed water molecules without any initial guidance. The formation of these "bonding clusters" (also called "iceberg layers") on surfaces is a fairly common phenomenon and does not affect the accessibility of the surface to other molecules, which is important for sensors [39]. The incorporation of an ordered layer of water into the interlayer slit affects the charge transfer between the C_2F and C_2OH surfaces (see Figure 2b) and affects the band gap for C_2F/C_2OH based structures (two-layer and bulk; see Figure 3c). The wavelength of the characteristic PL of C_2F/C_2OH-based structures in humid environments, estimated by Formula (1), is about 400 nm, which corresponds to the violet part of the visible light spectrum. The blueshift of the PL of structures based on C_2F/C_2OH in water and a humid environment makes it possible to use these compounds in humidity sensors, as well as to detect various chemical compounds in water. Note that the charge transfer (about -0.01 e^- per unit cell) shown in Figure 2c corresponds to the formation of C_2F–H_2O–C_2OH electrostatic bonds; therefore, C_2F/C_2OH interfaces can be considered stable in wet and liquid media. The smaller value of the charge transfer between the layers is caused by an increase in the distance between the layers and by significant changes in the charge density on water molecules (see Figure 2c). Note that the effect of water on the diamene-based sensors described in this section demonstrates the advantage of these compounds over lanthanide-based luminescent sensor materials, where coordination of active sites by water could quench the luminescence [7].

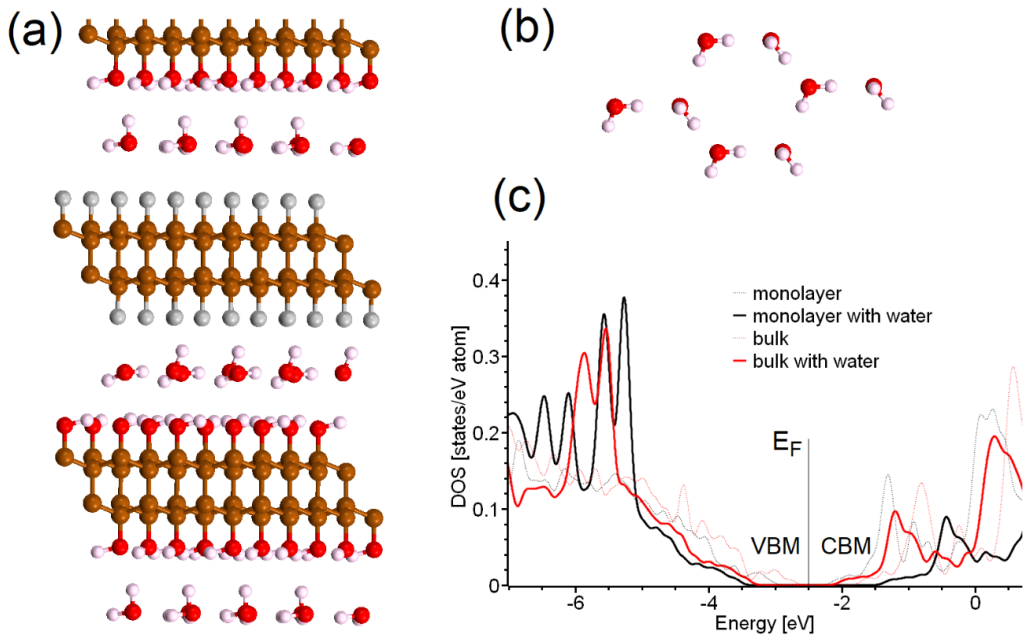

Figure 3. (**a**) Side view of optimized atomic structure of bulk C_2F/C_2OH system intercalated by water, and (**b**) top view of hexagonal patterns formed by water in the interlayer space of the structure presented in panel (**a**). (**c**) Total densities of states of C_2F/C_2OH single layer and bulk intercalated by water (solid lines), and total densities of states of corresponding structures without water. The color scale of the atoms in panel (**a**) is the same as in Figure 1.

3.3. Sensing Properties of C_2F/C_2OH Structures

The sensitivity of the optical properties of structures based on C_2F/C_2OH to a humid environment, considered in the previous section, demonstrates the possibility of using these materials as sensors. To explore this possibility, we modeled the detection of acetone (AC) in air and formaldehyde (FA) in water (see Figures 4a and 5a). Note that the termination of structures based on C_2F/C_2OH can be equally probable with a monolayer of C_2F or C_2OH. Thus, to complete the picture, we considered the adsorption of AC both on the C_2F-terminated side and on the C_2OH-terminated sides of the C_2F/C_2OH bilayers. The results of our calculations show that AC adsorption on both the fluorine and hydroxyl ends of the C_2F/C_2OH bilayer leads to a decrease in the calculated band gap from 1.2 to 0.7 eV. The last value, converted by Equation (1), corresponds to radiation in the red region of the spectrum. The enthalpy of adsorption of AC on the discussed substrate, calculated by Equation (3), is about −34 kJ/mol. Note that the magnitude of this value is close to the value of acetone vaporization enthalpy (about 32 kJ/mol at 300 K) [40]. Based on the formulas derived from our previous works (see, for example, Refs. [18,41]), the estimated temperature of the desorption of AC from C_2F/C_2OH is about 45 °C. Therefore, C_2F/C_2OH can be cleaned from adsorbed AC by simple mild heating. Thus, the redshift in C_2F/C_2OH fluorescent radiation may indicate the presence of AC in the air, and this therefore suggests that C_2F/C_2OH can be used in a device to detect the presence of AC in exhaled air. Note that a fairly small amount of material is required for the efficient operation of sensors of this type. As a rule, a thin layer of the material can be deposited on an area of the same order as the size of a focused excitation laser beam (3–5 μm), which is not overly intense, so that there is no heating of intercalating liquids or burning of a carbon substrate, and luminescence registration can be carried out for several minutes to accumulate signals in photon counting mode.

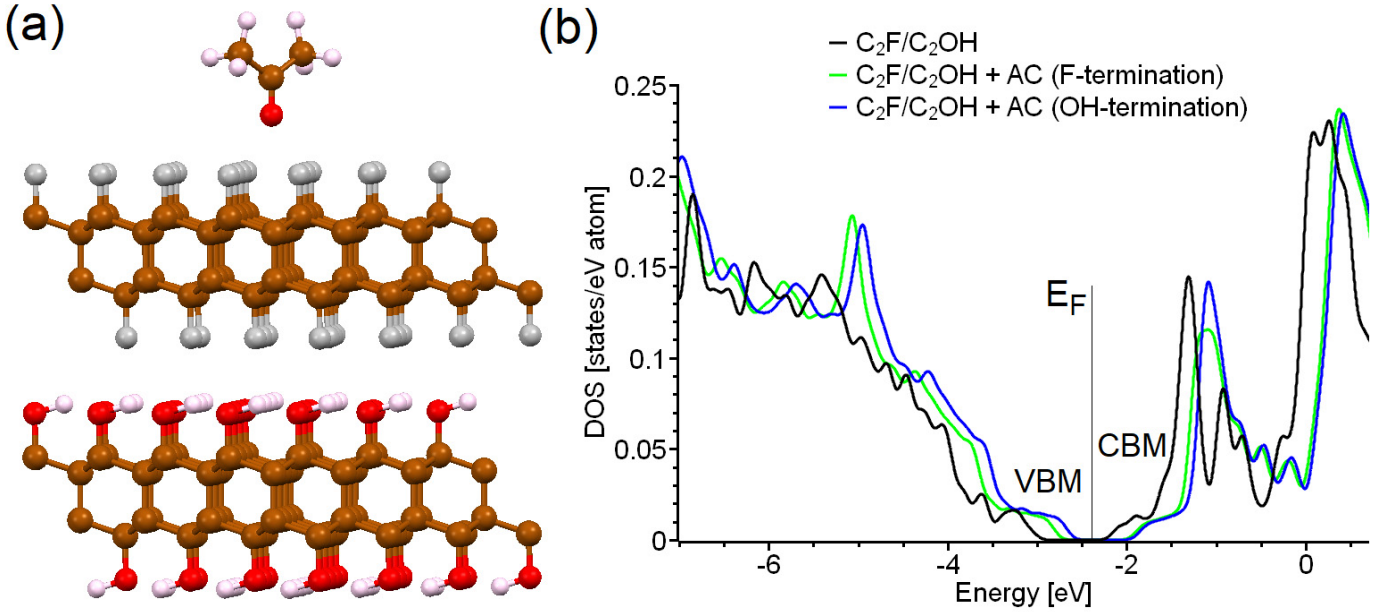

Figure 4. Side view of optimized atomic structure of C_2F/C_2OH single layer with acetone molecule physically adsorbed on F-terminated side (**a**), and total densities of states of the C_2F/C_2OH single layers before and after adsorption of acetone on different sides (terminations) (**b**). The color scale of the atoms in panel (**a**) is the same as in Figure 1.

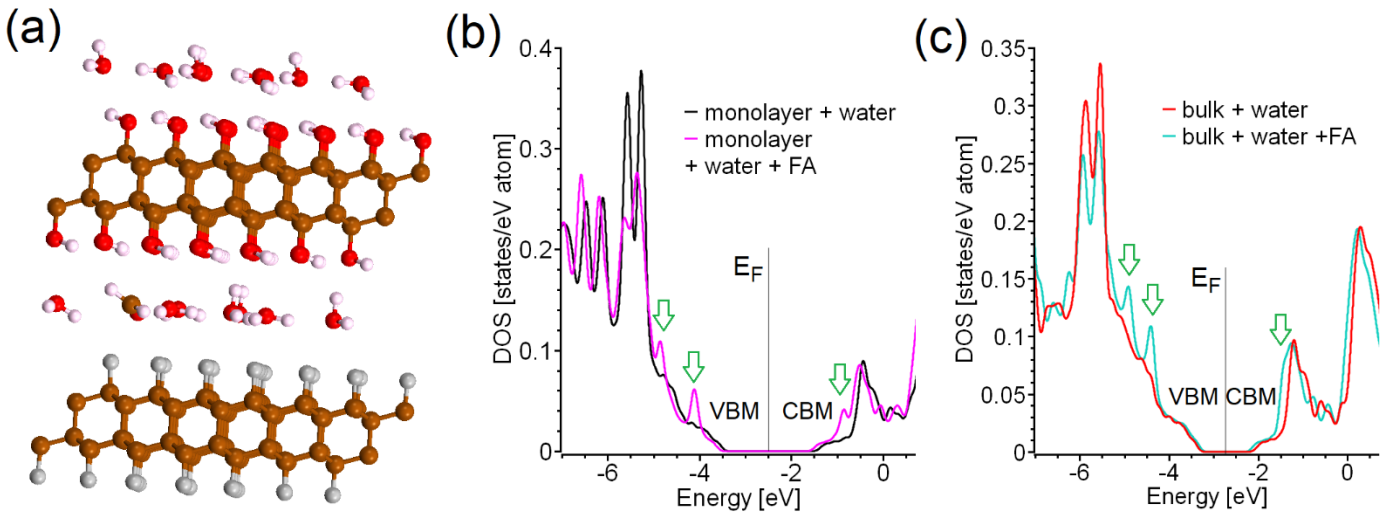

Figure 5. Side view of optimized atomic structure of bulk C_2F/C_2OH structure intercalated by water with molecule of formaldehyde (**a**), and total densities of states of C_2F/C_2OH single layer intercalated by water (**b**) and bulk intercalated by water (**c**) with and without molecules of formaldehyde (see panel (**a**)). The arrows show features in electronic structure corresponding with additional adsorption in near-UV part of spectra. The color scale of the atoms in panel (**a**) is the same as in Figure 1.

To evaluate the sensor properties of the systems based on C_2F/C_2OH in liquid media, we simulated the interaction of formaldehyde (FA) molecules with bulk and bilayer C_2F/C_2OH systems intercalated with water. We started our modeling by replacing one water molecule with a single FA molecule in the already-simulated bulk and layered structures with an intercalated water layer and then carried out a full optimization of lattice constants and atomic positions. The results of our calculations demonstrate that the presence of a single FA molecule does not significantly affect the order of water molecules (compare Figure 5a with Figure 3a). In contrast to AC adsorption from air, the interaction of FA with the C_2F/C_2OH structure dissolved in water does not lead to a change in the band gap either in bulk or in two-layer C_2F/C_2OH (see Figure 5b,c). However, there are two distinct peaks near VBM and one distinct peak near CBM. These three peaks can be the sources of two additional features in the absorption spectra of C_2F/C_2OH in the near UV region of the spectrum, and C_2F/C_2OH can thus be used for simple optical detection of FA in water, by analogy with the previously discussed MOF-based method. [18]. Unlike the detection of molecules by detecting changes in the spectrum (color) of emitted fluorescent radiation, the detection of molecules by detecting changes in the absorption spectrum of the supporting active nanomaterial (matrix) requires more effort in sample preparation for its use in sensor devices in order to provide appropriate changes in the intensity of the light transmitted through a matrix with guest molecules.

The final step of our work was to compare the proposed material with previously reported carbon-based sensing systems. Graphene-based compounds are usually discussed as the best prospective materials for carbon-based sensing materials, mainly due to the changes in their conductivity and in the spectrum of electronic states during the sorption of external agents by means of van der Waals forces, because they have a zero gap and are essentially semimetals in the initial state. In contrast, sensors based on graphene oxide or reduced graphene oxide have a large nonzero gap (~2.2 eV or 1~1.7 eV, depending upon the degree of reduction). This makes it possible to use the fluorescence of these materials for the detection of agents that have the properties of luminescence quenchers [42]. Among the latter are the cations of a number of metals. The same applies to the grafting onto graphene oxide particles of sensitive fluorescent organic molecules that can effectively interact with the analyte and whose intrinsic luminescence is not suppressed by a wide-gap carrier particle [42]. Nanoscale graphene quantum dots also have a gap and exhibit photoluminescent properties that can be used to detect luminescence quenching agents in

trace amounts. Graphene quantum dots are sometimes used in combination with other metal nanoparticles to study the analyte by measuring the optical absorption of the solution and detecting the spectral shifts associated with plasmon resonance and the presence of the analyte [43]. The main advantage of the described systems over the proposed C_2F/C_2OH system is the developed procedure of the production. The main disadvantage of other carbon-based materials is that the exact atomic and electronic structure of the materials is uncontrollable.

4. Conclusions

Based on the results of ab initio modeling, we conclude that layered compounds built from C_2F/C_2OH interfaces are stable in air and water. This paper also demonstrates the possibility of UV light conversion into visible light, as in the case of light-emitting carbon dots. The adsorption of acetone molecules from the air changes the spectral composition of emitted radiation from orange-yellow to red. On the contrary, intercalation with water leads to a blueshift in the luminescence to the violet region of the spectrum. These results demonstrate that C_2F/C_2OH-based thin-layer materials have a unique optical response selectivity for different types of analytes. In contrast to adsorption from the gas phase, the presence of a formaldehyde molecule in water on or between the layers of materials based on C_2F/C_2OH does not change the color of the emitted light, but changes their absorption spectra in the near-ultraviolet spectral range. Therefore, C_2F/C_2OH-based materials can also be proposed as materials for the detection of various simple molecules in both gaseous and liquid media.

Author Contributions: Conceptualization, D.W.B. and V.Y.O.; methodology, D.W.B.; software, D.W.B.; validation, D.W.B., V.Y.O.; formal analysis, D.W.B.; investigation, D.W.B.; resources, D.W.B.; data curation, V.Y.O.; writing—original draft preparation, D.W.B.; writing—review and editing, V.Y.O.; visualization, D.W.B.; funding acquisition, D.W.B. and V.Y.O. All authors have read and agreed to the published version of the manuscript.

Funding: D.W.B. was funded by Russian Science Foundation (project no. 21-12-00392). V.Yu.O. was funded by the Ioffe Institute (project no. 0040-20140013).

Institutional Review Board Statement: Not applicable.

Informed Consent Statement: Not applicable.

Data Availability Statement: Data available on request due to restrictions eg privacy or ethical.

Acknowledgments: D.W.B. acknowledges the support of the Russian Science Foundation (project no. 21-12-00392). V.Yu.O. acknowledges the support of the Ioffe Institute (project no. 0040-2014-0013).

Conflicts of Interest: The authors declare no conflict of interest.

References

1. Venkateswarulu, M.; Gaur, P.; Koner, R.R. Sensitive molecular optical material for signaling primary amine vapors. *Sens. Actuators B Chem.* **2015**, *210*, 144–148. [CrossRef]
2. Silva, A.P.; Fox, D.B.; Huxley, A.J.M.; Moody, T.S. Current developments in fluorescent PET (photoinduced electron transfer) sensors and switches. *Coord. Chem. Rev.* **2000**, *205*, 41–57. [CrossRef]
3. Mader, H.S.; Wolfbeis, O.S. Optical ammonia sensor based on upconverting luminescent nanoparticles. *Anal Chem.* **2010**, *82*, 5002–5004. [CrossRef] [PubMed]
4. Mukherjee, S.; Betal, S.; Chattopadhyay, A.P. Luminescence sensing, DFT, extraction and monitoring of Cr^{3+} and Al^{3+}via the application of first derivative fluorescence spectroscopy. *New J. Chem.* **2020**, *44*, 12692–12703. [CrossRef]
5. Chai, B.-L.; Yao, S.-L.; Xie, X.; Xu, H.; Zheng, T.-F.; Li, J.-Y.; Chen, J.-L.; Liu, S.-J.; Wen, H.-R. Luminescent Metal–Organic Framework-Based Fluorescence Turn-On and Red-Shift Sensor toward Al3+ and Ga3+: Experimental Study and DFT Calculation. *Cryst. Growth Des.* **2022**, *22*, 277–284. [CrossRef]
6. Vellingiri, K.; Boukhvalov, D.W.; Pandey, S.K.; Deep, A.; Kim, K.H. Luminescent metal-organic frameworks for the detection of nitrobenzene in aqueous media. *Sens. Actuators B Chem.* **2017**, *245*, 305–313. [CrossRef]
7. Aulsebrook, M.L.; Graham, B.; Grace, M.R.; Tuck, K.L. Lanthanide complexes for luminescence-based sensing of low molecular weight analytes. *Coord. Chem. Rev.* **2018**, *375*, 191–220. [CrossRef]

8. Timmer, B.; Olthuis, W.; van den Berg., A. Ammonia sensors and their applications—A review. *Sens. Actuators. B Chem.* **2005**, *107*, 666–677. [CrossRef]
9. Roy, S.; Chakraborty, A.; Maji, T.K. Lanthanide–organic frameworks for gas storage and as magneto-luminescent materials. *Coord. Chem. Rev.* **2014**, *273–274*, 139–164. [CrossRef]
10. Fujisaku, T.; Igarashi, R.; Shirakawa, M. Nanometre-scale visualization of chemical parameter changes by T1-weighted ODMR imaging using a fluorescent nanodiamond. *Chemosensors* **2020**, *8*, 68. [CrossRef]
11. Kočí, M.; Kromka, A.; Bouřa, A.; Szabó, O.; Husák, M. Hydrogen-terminated diamond surface as a gas sensor: A comparative study of its sensitivities. *Sensors* **2021**, *21*, 5390. [CrossRef]
12. Dettenrieder, C.; Türkmen, D.; Mattsson, A.; Österlund, L.; Karlsson, M.; Mizaikoff, B. Determination of Volatile Organic Compounds in Water by Attenuated Total Reflection Infrared Spectroscopy and Diamond-Like Carbon Coated Silicon Wafers. *Chemosensors* **2020**, *8*, 75. [CrossRef]
13. da Silva, Á.R.L.; de Araujo, D.M.; da Silva, E.B.S.; Vieira, D.S.; Monteiro, N.D.K.V.; Martinez-Huitle, C.A. Understanding the behavior of caffeine on a boron-doped diamond surface: Voltammetric, DFT, QTAIM and ELF studies. *New J. Chem.* **2017**, *41*, 7766–7774. [CrossRef]
14. Yuan, X.; Gao, N.; Gao, X.; Qiu, D.; Xu, R.; Sun, Z.; Jiang, Z.; Liu, J.; Li, H. Nanopyramid boron-doped diamond electrode realizing nanomolar detection limit of 4-nonylphenol. *Sens. Actuators B Chem.* **2019**, *281*, 830–836. [CrossRef]
15. Leenaerts, O.; Partoens, B.; Peeters, F.M. Hydrogenation of bilayer graphene and the formation of bilayer graphane from first principles. *Phys. Rev. B* **2009**, *80*, 245422. [CrossRef]
16. Barboza, A.P.M.; Guimaraes, M.H.D.; Massote, D.V.P.; Campos, L.C.; Barbosa Neto, N.M.; Cancado, L.G.; Lacerda, R.G.; Chacham, H.; Mazzoni, M.S.C.; Neves, B.R.A. Room-temperature compression-induced diamondization of few-layer graphene. *Adv. Mater.* **2011**, *23*, 3014. [CrossRef]
17. Bakharev, P.V.; Huang, M.; Saxena, M.; Lee, S.W.; Joo, S.H.; Park, S.O.; Dong, J.; Camacho-Mojica, D.C.; Jin, S.; Kwon, Y.; et al. Chemically induced transformation of chemical vapour deposition grown bilayer graphene into fluorinated single-layer diamond. *Nat. Nanotechnol.* **2020**, *15*, 59–66. [CrossRef]
18. Lavini, F.; Rejhon, M.; Reido, E. Two-dimensional diamonds from sp2-to-sp3 phase transitions. *Nat. Rev. Mater.* **2022**, *7*, 814–832. [CrossRef]
19. Martins, L.G.P.; Matos, M.J.S.; Paschoal, A.R.; Freire, P.T.C.; Andrade, N.F.; Aguiar, A.L.; Kong, J.; Neves, B.R.A.; de Oliveira, A.B.; Mazzoni, M.S.C.; et al. Raman evidence for pressure-induced formation of diamondene. *Nat. Comm.* **2017**, *8*, 96. [CrossRef]
20. BenMouss, A.; Soltani, A.; Schühle, U.; Haenen, K.; Chong, Y.M.; Zhang, W.J.; Hochedez, J.F. Recent developments of wide-bandgap semiconductor based UV sensors. *Diam. Rel. Mater.* **2009**, *18*, 860–864. [CrossRef]
21. Pearton, S.J.; Ren, F.; Yu-Lin Wang, Y.-L.; Chu, B.H.; Chen, K.H.; Chang, C.Y.; Lim, W.; Lin, J.; Norton, D.P. Recent advances in wide bandgap semiconductor biological and gas sensors. *Prog. Mater. Sci.* **2010**, *55*, 1–59. [CrossRef]
22. Saasa, V.; Malwela, T.; Beukes, M.; Mokgotho, M.; Liu, C.-P.; Mwakikunga, B. Sensing Technologies for Detection of Acetone in Human Breath for Diabetes Diagnosis and Monitoring. *Diagnostics* **2018**, *8*, 12. [CrossRef] [PubMed]
23. Vellingiri, K.; Deep, A.; Kim, K.-H.; Boukhvalov, D.W.; Kumar, P.; Yao, Q. The sensitive detection of formaldehyde in aqueous media using zirconium-based metal organic frameworks. *Sens. Actuators B: Chem.* **2017**, *241*, 938–948. [CrossRef]
24. Soler, J.M.; Artacho, E.; Gale, J.D.; Garsia, A.; Junquera, J.; Orejon, P.; Sanchez-Portal, D. The SIESTA Method for Ab-Initio Order-N Materials Simulation. *J. Phys. Condens. Matter.* **2002**, *14*, 2745. [CrossRef]
25. Perdew, J.P.; Burke, K.; Ernzerhof, M. Generalized Gradient Approximation Made Simple. *Phys. Rev. Lett.* **1996**, *77*, 3865. [CrossRef]
26. Dion, M.; Rydberg, H.; Schröder, E.; Langreth, D.C.; Lundqvist, B.I. Van der Waals density functional for general geometries. *Phys. Rev. Lett.* **2004**, *92*, 246401. [CrossRef]
27. Troullier, O.N.; Martins, J.L. Efficient Pseudopotentials for Plane-Wave Calculations. *Phys. Rev. B* **1991**, *43*, 1993. [CrossRef]
28. Mentel, M.; Baerends, E.J. Can the Counterpoise Correction for Basis Set Superposition Effect Be Justified? *J. Chem. Theory Comput.* **2014**, *10*, 252–267. [CrossRef]
29. Gutowski, M.; Grzegorz Chałasiński, G. Critical evaluation of some computational approaches to the problem of basis set superposition error. *J. Chem. Phys.* **1993**, *98*, 5540–5554. [CrossRef]
30. van Schilfgaarde, M.; Kotani, T.; Faleev, S. Quasiparticle Self-Consistent GW Theory. *Phys. Rev. Lett.* **2006**, *96*, 226402. [CrossRef]
31. Tian, L.; Chen, F.; Ding, H.; Li, X.; Li, X. The influence of inorganic electrolyte on the properties of carbon quantum dots in electrochemical exfoliation. *J. Electrochem. Soc.* **2020**, *878*, 114673. [CrossRef]
32. Ding, M.; Xiao, R.; Zhao, C.; Bukhvalov, D.; Chen, Z.; Xu, H.; Tang, H.; Xu, J.; Yang, X. Evidencing Interfacial Charge Transfer in 2D CdS/2D MXene Schottky Heterojunctions toward High-Efficiency Photocatalytic Hydrogen Production. *Solar Rrl* **2021**, *5*, 2000414. [CrossRef]
33. Boukhvalov, D.W.; Dreyer, D.R.; Bielawski, C.W.; Son, Y.-W. A Computational Investigation of the Catalytic Properties of Graphene Oxide: Exploring Mechanisms by using DFT Methods. *ChemCatChem* **2012**, *4*, 1844–1849. [CrossRef]
34. Perrin, C.L.; Nielson, J.B. "Strong" hydrogen bonds in chemistry and biology. *Ann. Rev. Phys. Chem.* **1997**, *48*, 511–544. [CrossRef] [PubMed]
35. Spanu, L.; Sorella, S.; Galli, G. Nature and strength of interlayer binding in graphite. *Phys. Rev. Lett.* **2009**, *103*, 196401. [CrossRef] [PubMed]

36. Kim, J.-S.; Choi, J.S.; Lee, M.J.; Park, B.H.; Boukhvalov, D.W.; Son, Y.-W.; Yoon, D.; Cheong, H.; Park, J.Y.; Salmeron, M. Between Scylla and Carbides: Hydrophobic Graphene-Guided Water Diffusion on Hydrophilic Substrates. *Sci. Rep.* **2013**, *3*, 2309. [CrossRef]
37. Zheng, Y.; Su, C.; Lu, J.; Loh, K.P. Room-Temperature Ice Growth on Graphite Seeded by Nano-Graphene Oxide. *Angew. Chem.* **2013**, *125*, 8870–8874. [CrossRef]
38. 30 Boukhvalov, D.W.; Katsnelson, M.I.; Son, Y.-W. Origin of anomalous water permeation through graphene oxide membrane. *Nano Lett.* **2013**, *13*, 3930–3935. [CrossRef]
39. Wakisaka, A.; Shimizu, Y.; Nishi, N.; Tokumaru, K.; Sakuragi, H. Interaction of hydrophobic molecules with water influenced by the clustering conditions of acetonitrile–water mixtures. *J. Chem. Soc. Faraday Trans.* **1992**, *88*, 1129–1135. [CrossRef]
40. NIST Chemistry Webbook. Available online: https://webbook.nist.gov/cgi/cbook.cgi?ID=C67641&Mask=4 (accessed on 29 October 2022).
41. Bondino, F.; Duman, S.; Nappini, S.; D'Olimpio, G.; Ghica, C.; Menteş, T.O.; Politano, A. Improving the efficiency of gallium telluride (GaTe) for photocatalysis, electrocatalysis, and chemical sensing through defects engineering and interfacing with its native oxide. *Adv. Funct. Mater.* **2022**, *32*, 2205923. [CrossRef]
42. Sivasubramanian, S.; David, C.I.; Prabhu, J.; Raju, N. Functionalized graphene oxide materials for fluorometric sensing of various analytes: A mini review. *Mater. Adv.* **2021**, *2*, 6197–6212. [CrossRef]
43. Babazadeh, S.; Moghaddam, P.A.; Keshipour, S.; Mollazade, K. Colorimetric sensing of imidacloprid in cucumber fruits using a graphene quantum dot/Au (III) chemosensor. *Sci. Rep.* **2020**, *10*, 14327. [CrossRef] [PubMed]